Journal of Materials Chemistry B

Accepted Manuscript

ROYAL SOCIETY OF CHEMISTRY

www.rsc.org/materialsB

Journal of Materials Chemistry B

PAPER

Activated macrophage-targeted dextran–methotrexate/folate conjugate prevents deterioration of collagen-induced arthritis in mice

Received 00th January 20xx,
Accepted 00th January 20xx

DOI: 10.1039/x0xx00000x

www.rsc.org/

Modi Yang,[a] Jianxun Ding,*[b] Ying Zhang,[b] Fei Chang,*[c] Jincheng Wang,[c] Zhongli Gao,*[a] Xiuli Zhuang[b] and Xuesi Chen[b]

Rheumatoid arthritis (RA) is an autoimmune inflammatory disease along with articular synovial hyperplasia, cartilage destruction, and bone erosion. In RA pathophysiology, the activated macrophages contribute to the initiation and maintenance of the disease. Folate receptor, an overexpressed receptor on the activated macrophages, becomes a promising target site for RA treatment. In this work, the folate-modified dextran–methotrexate conjugate (noted as Dex-*g*-MTX/FA) was synthesized with the untargeted dextran–methotrexate prodrug (referred as Dex-*g*-MTX) as control. The two prodrugs self-assembled into spherical micelles with both scales of about 90 nm and exhibited sustained MTX release. Dex-*g*-MTX/FA exhibited more superior cellular uptake mediated by folate receptor and higher cytotoxicity toward the macrophages activated by lipopolysaccharide (LPS) compared with Dex-*g*-MTX. Moreover, Dex-*g*-MTX/FA possessed improved biodistribution in lesion site and stronger remission of RA through the inhibition of proinflammatory cytokines in comparison with both Dex-*g*-MTX and free MTX. These results demonstrated that the folate-targeted prodrug, *i.e.*, Dex-*g*-MTX/FA, is a potential strategy for the activated macrophage-targeted therapy of RA.

1 Introduction

Rheumatoid arthritis (RA), as a chronic autoimmune disease, always gives rise to synovitis, cartilage destruction, and bone erosion in clinic.[1,2] So far, the pathogenesis of RA is not extremely clear. However, there is a definitely obvious correlation between the recruitment of multiple potent mediators, including proinflammatory cytokines (*e.g.*, tumor necrosis factor-α (TNF-α), interleukin-1β (IL-1β), and interleukin-6 (IL-6)), chemokines, and metalloproteinases, and so on, and the progress level of disease. It is widely shared that the activated macrophages, which are the most common phenotype in RA,[3] as the main source of various inflammatory mediators, are the key effectors in the development of RA.[4] Many receptors are specifically expressed on the activated macrophages, for instance, folate receptor (FR)[5–7] and scavenger receptor,[8] which are not on the nonactivated macrophages or normal cells. Therefore, the activated macrophages have become a primary target for active targeting therapy of RA.[4,9]

FR is a kind of anchored proteins expressed on cell surface, which has high affinity to folic acid (FA).[10] FR family is made up of four subtypes, including FRα, FRβ, FRγ, and FRδ,[10] and each has different biodistribution. Many researches revealed that FRα is the dominant subtype for tumor-targeted treatment. Nevertheless, FRβ specifically overexpressed on the surface of activated macrophages was also demonstrated in the patients with RA.[11] Another study reported that FR, which overexpressed on the synovial macrophages in the rat of experimental arthritis, possessed higher affinity for binding folate conjugates compared with FR on normal macrophages.[5,6] Consequently, the specificity of expression and biodistribution of FR in the activated macrophages make FR become a potential receptor for active targeting therapy of RA.[12–15]

Methotrexate (MTX) was early prescribed for antitumor treatment through the blockage of nucleotide synthesis and cell proliferation. In recent 20 years, MTX as the disease-modifying antirheumatic drug (DMARD) has been the first-line medicine for either monotherapy or combination with other biologics. MTX exhibits excellent inhibitory efficacy on the production of proinflammatory cytokines and delays the disease progression in the affected joints.[16] Unfortunately, a portion of patients exhibited tolerance to long-time administration of MTX, and the others suffered from severe side effects, including suppression of bone marrow, damage to liver and kidney, dysfunction of gastrointestinal tract, *etc.*, for the general distribution of MTX.[17] The specific delivery of MTX to the lesion cells and obstruction of normal cells from uptaking the drug may validly address these issues.

Dextran (Dex) is a sort of polysaccharides. For its excellent biological properties, such as favorable biocompatibility,

[a] Department of Orthopedics, China-Japan Union Hospital of Jilin University, Changchun 130033, P. R. China. E-mail: zhongliqao@sina.com
[b] Key Laboratory of Polymer Ecomaterials, Changchun Institute of Applied Chemistry, Chinese Academy of Sciences, Changchun 130022, P. R. China. E-mail: jxding@ciac.ac.cn
[c] Department of Orthopedics, The Second Hospital of Jilin University, Changchun 130041, P. R. China. E-mail: ccfei_cn@hotmail.com
† Footnotes relating to the title and/or authors should appear here.
Electronic Supplementary Information (ESI) available: See DOI: 10.1039/x0xx00000x

biodegradability, and polyfunctionality, Dex as an ideal biomaterial is widely applied for tissue engineering and therapeutic agent delivery.[18,19] Chemical conjugation as one of the most promising approaches is beneficial to the combination of drugs and nanocarriers, and the production of efficient prodrugs.[20] In this study, a FA-targeted Dex–MTX conjugate, that is, Dex-*g*-MTX/FA, and untargeted MTX prodrug, *i.e.*, Dex-*g*-MTX, were synthesized, and then were systematically characterized for their physiochemical properties. The properties of Dex-*g*-MTX/FA targeting to the activated macrophages was investigated *in vitro* using RAW 264.7 cell line. The biodistribution and anti-inflammatory efficacy *in vivo* were finally performed in collagen-induced arthritis (CIA) in mice.

2 Materials and methods

2.1 Materials

FA and Dex (number-average molecular weight (M_n) = 5000 g/mol) were purchased from J&K scientific Ltd. (Beijing, P. R. China). MTX was obtained from Beijing Huafeng United Technology Co., Ltd. (Beijing, P. R. China). 1-Ethyl-(3-(dimethylamino)propyl) carbodiimide hydrochloride (EDC·HCl) and 4-*N*,*N*-dimethylaminopyridine (DMAP) were acquired from GL Biochem Co., Ltd. (Shanghai, P. R. China). Cell culture substrates, including Dulbecco's modified Eagle's medium (DMEM) and fetal bovine serum (FBS), were bought from Gibco (NY, Grand Island, USA). Penicillin and streptomycin were purchased from Huabei Pharmaceutical Co., Ltd. (Shijiazhuang, P. R. China). Lipopolysaccharide (LPS) was obtained from Biosharp Co. (Hefei, P. R. China). 4′,6-Diamidino-2-phenylindole dihydrochloride (DAPI) and fluorescein isothiocyanate (FITC) were obtained from Sigma-Aldrich (Shanghai, P. R. China). Bovine type II collagen (BCol II) (2.0 mg/mL), complete Freund's adjuvant (CFA) (2.0 mg/mL), and incomplete Freund's adjuvant (IFA) were purchased from Chondrex (Washington, USA). The antibodies of anti-TNF-α, anti-IL-1β, and anti-IL-6 were purchased from Abcam (Cambridge, MA, USA). The primers of TNF-α, IL-1β, IL-6, and housekeeping gene GADPH were bought from Sangon Biotech (Shanghai, P. R. China). The reverse transcription kit and SYBR Premix Ex Taq™ kit were purchased from Takara Biomedical Technology (Beijing, P. R. China). The commercial enzyme-linked immunosorbent assay (ELISA) kits of TNF-α, IL-1β, and IL-6 were purchased from R&D Systems (Minneapolis, MN, USA).

2.2 Syntheses of Dex-*g*-MTX/FA and Dex-*g*-MTX

Dex-*g*-MTX/FA was synthesized through a one-step condensation reaction with EDC·HCl as a condensing agent and DMAP as a catalyst (Scheme 1). Typically, Dex (10.0 g, 61.7 mmol glucose units) was first dissolved in 50.0 mL MilliQ water, and then MTX (448.8 mg, 0.99 mmol) and FA (109.0 mg, 0.25 mmol) in 50.0 mL of dimethyl sulfoxide (DMSO) was dropwise added into Dex aqueous solution. The reaction was proceeded at room temperature for 72 h, and the final solution was dialyzed against Milli-Q water (molecular weight cut-off (MWCO) = 3500 Da). The white flocculent solid was obtained after lyophilization with a high yield of appropriate 90%. Dex-*g*-MTX was synthesized with the reactants of Dex and MTX through the same above protocol. The yield was also above 90%.

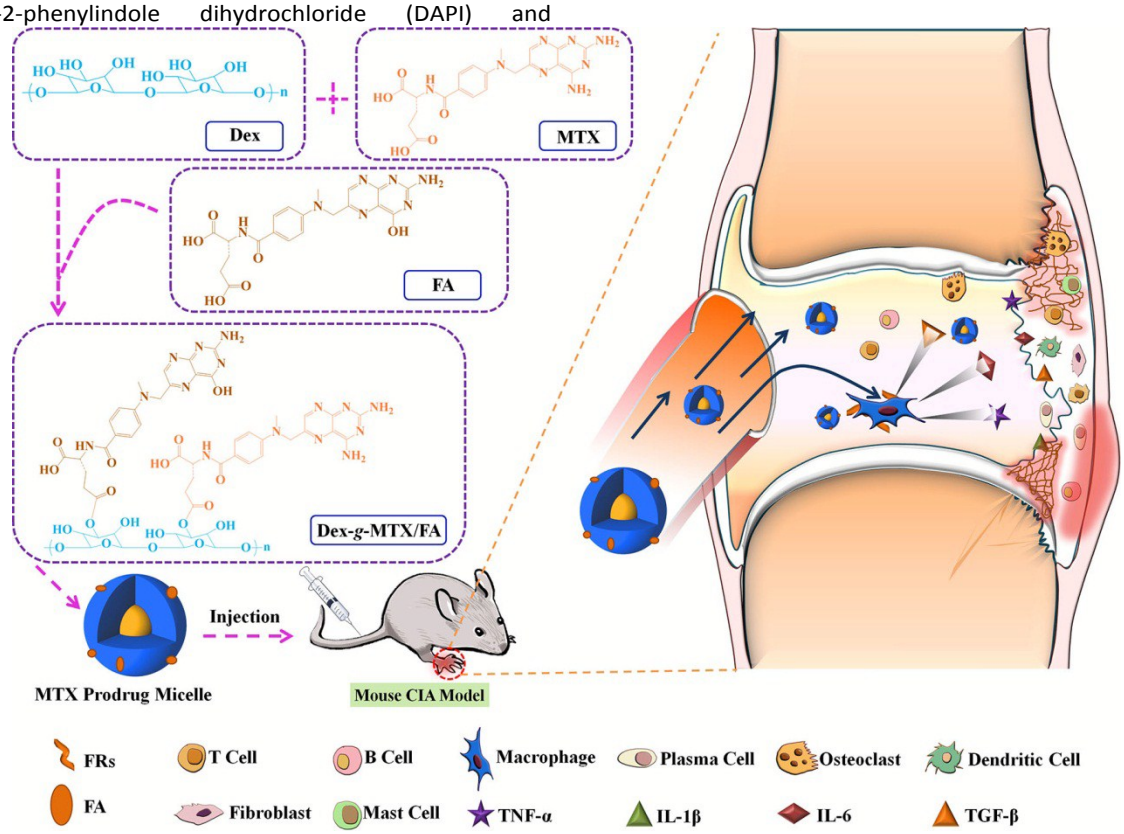

Scheme 1 Schematic illustration of synthesis, intravenous administration, targeted delivery, and brief mechanism of Dex-*g*-MTX/FA in treatment of CIA.

2.3 Measurements

Proton nuclear magnetic resonance (^{1}H NMR) spectra were detected by a Bruker AV 600 NMR spectrometer (Billerica, MA, USA) in a mixed solvent of deuterated water (D_2O) and deuterated dimethyl sulfoxide (DMSO-d_6). Fourier-transform infrared (FT-IR) spectra were measured *via* a Bio-Rad Win-IR instrument (Bio-Rad Laboratories Inc., Cambridge, MA, USA) using potassium bromide method. Transmission electron microscopy (TEM) measurements were carried out by a JEM-1011 transmission electron microscope (JEOL, Tokyo, Japan) with an accelerating voltage of 100 kV. The prodrug micelle samples were prepared by being directly dissolved in 0.001 M phosphate-buffered saline (PBS), and then carefully dropped on a carbon-coated copper grid and dried at room temperature in the air. The hydrodynamic diameters (D_hs) of conjugate micelles were measured by dynamic laser scattering (DLS) measurements with a vertically polarized He-Ne laser (DAWN EOS, Wyatt Technology Co., Santa Barbara, CA, USA). The critical micelle concentrations (CMCs) of Dex-*g*-MTX/FA and Dex-*g*-MTX were detected by fluorophotometry using Nile Red as a probe. The MTX and FA contents in Dex-*g*-MTX/FA and Dex-*g*-MTX were detected by an ultraviolet-visible (UV-Vis) spectrophotometry with λ_{ab} = 303 nm (UV-1800, Shimadzu, Kyoto, Japan).

2.4 Hemolysis tests

The hemocompatibility of Dex-*g*-MTX/FA, Dex-*g*-MTX, and free MTX was evaluated by a spectrophotometry technique. Initially, the fresh rabbit blood was extracted from the heart of rabbit. Subsequently, the isolation of red blood cells (RBCs) was performed by centrifugation at 2500 rpm for 15 min. After careful wash, the solutions of three MTX formulations, that is, Dex-*g*-MTX/FA, Dex-*g*-MTX, or free MTX, with varied concentrations were added to the 2% (*V*/*V*) RBCs. After mixing by vortex, the suspensions of RBCs with different concentrations of MTX formulations were incubated at 37 °C in a thermostatic water bath for 3 h. Normal saline (NS) and Triton X-100 at a concentration of 1 × 10^4 mg/mL that could lyse RBCs were acted as negative and positive controls, respectively. Later on, the suspensions of RBCs were centrifuged at 3000 rpm for 10 min. 100.0 μL of the supernatant of every sample was added to a 96-well plate. The free hemoglobin released from RBCs was detected on a Bio-Rad 680 microplate reader at 540 nm. The hemolysis ratio was calculated using Equation (2).

$$\text{Hemolytic ratio}\,(\%) = \frac{A_{\text{sample}} - A_{\text{negative control}}}{A_{\text{positive control}} - A_{\text{negative control}}} \times 100 \quad (2)$$

Where, A_{sample}, $A_{\text{negitive control}}$, and $A_{\text{positive control}}$ presented the absorbances of sample, and negative and positive controls, respectively.

2.5 *In vitro* drug release

Dex-*g*-MTX/FA or Dex-*g*-MTX was dispersed in PBS at pH 7.4, transferred into a dialysis bag (MWCO = 3500 Da), and then put them into 100.0 mL of PBS contained 5% (*V*/*V*) Tween 80 at 37 °C with persistent shaking of 70 rpm. At the pre-established time point, 2.0 mL of release medium was taken out, and an equal volume of fresh solution was added to the system. The amount of released MTX was measured by a UV-Vis spectrophotometer with λ_{ab} = 303 nm.

2.6 Cellular uptake studies

RAW 264.7 cells were cultured in complete DMEM medium containing 10% (*V*/*V*) FBS and 1% (*W*/*V*) penicillin-streptomycin at 37 °C in humidified 5% (*V*/*V*) carbon dioxide (CO_2) atmosphere for 12 h. Cells were activated with 20.0 ng/mL LPS for 48 h. After cell activation, the original medium was replaced with the FITC-labeled Dex-*g*-MTX/FA or Dex-*g*-MTX solution in DMEM at a final MTX concentration of 20.0 μg/mL followed by incubation for another 2 h.

2.5.1 Confocal Laser Scanning Microscope (CLSM). The activated and nonactivated cells on glass coverslips cocultured with the two labeled conjugates were washed three times with PBS and fixed with 4% (*W*/*V*) PBS-buffered formaldehyde for 30 min at room temperature. Subsequently, the staining of cell nucleus was performed with DAPI (blue) for 3 min. The microimage of cellular uptake was finally taken under a LSM 780 CLSM (Carl Zeiss, Jena, Germany) with 10 × eyepiece and 60 × objective.

2.5.2 Flow Cytometry (FCM). In addition, the activated and nonactivated cells cocultured with the two stained conjugates were washed three times with PBS. Then, the cells were harvested *via* centrifugation for 5 min at 1500 rpm, 4 °C. For removing the redundant fluorescence, the cells were suspended and washed with PBS for two times again. After that, the cells were finally suspended with 500.0 μL of PBS. The fluorescence intensity of cellular uptake was detected by FCM (Beckman, California, USA).

2.7 Cytotoxicity assays

The cytotoxicity of Dex-*g*-MTX/FA, Dex-*g*-MTX, and free MTX was detected by a MTT assay toward RAW 264.7 cells. Cells were activated by LPS with 20.0 ng/mL for 48 h, and then seeded in 96-well plates with a density of 8000 cells per well for 12 h. And then, the cell culture medium was refreshed with 200.0 μL of medium containing Dex-*g*-MTX/FA, Dex-*g*-MTX, or free MTX at various MTX equivalent concentrations from 4.9 ng/mL to 20.0 μg/mL. The cells were incubated for another 72 h. After that, 100.0 μL of MTT solution containing 0.05 mg of MTT was added and incubated for further 4 h. Subsequently, the medium was replaced with 100.0 μL of DMSO. Finally, the absorbance of solution in each well was measured on a Bio-Rad 680 microplate reader (Hercules, CA, USA) at 490 nm. The cell viability was calculated in accordance with Equation (1).

$$\text{Cell viability}\,(\%) = \frac{A_{\text{sample}}}{A_{\text{control}}} \times 100 \quad (1)$$

2.8 *Ex vivo* tissue distribution assessments

In this work, all animals were handled under the protocol approved by the Institutional Animal Care and Use Committee of Jilin University. Typically, DBA/1J mice were maintained in 12 h light/12 h dark cycles with continuous access to food and water. CIA was induced in male DBA/1J mice of 8 – 10 weeks old. To induce CIA, mice were injected at the base of the tail intradermally with 100.0 μg of BCol II (2.0 mg/mL) emulsified

in 50.0 μL of CFA (2.0 mg/mL). As shown in Scheme 2, it was followed by a booster immunization 21 days later with BCol II emulsified in IFA. At 48 days after primary immunization, the FITC-labeled Dex-*g*-MTX/FA, Dex-*g*-MTX, or MTX was injected into the tail vein of CIA mice with a MTX equivalent dose of 5.0 mg per kg body weight (mg/(kg BW)). NS was injected as control. The mice were sacrificed at 12 h post-injection. The affected joints were excised immediately and subsequently washed with NS three times for *ex vivo* imaging of FITC fluorescence on a Maestro 500FL *in vivo* Imaging System (Cambridge Research & Instrumentation, Inc., USA). Moreover, the signals were also quantitatively analyzed using a Maestro™ 2.4 software.

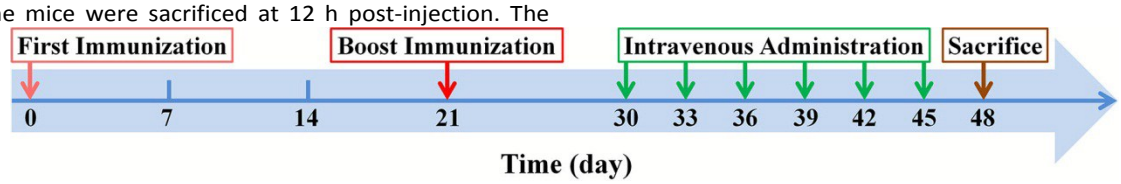

Scheme 2 Time axis of animal experimental progress.

2.9 Therapeutic efficacy evaluations *in vivo*

The CIA mice were induced by the above protocol. The CIA mice were administrated through the intravenous injection of 200.0 μL of Dex-*g*-MTX/FA, Dex-*g*-MTX, or MTX solutions in NS at a MTX equivalent dose of 5.0 mg/(kg BW) with NS as control once every three days (n = 6 for each group). The mice were examined every three days after administration for the signs of joint inflammation and scored as follows: 0 = normal, 1 = mild swelling and erythema confined to the tarsals or ankle joint, 2 = mild swelling and erythema extending from the ankle to tarsus, 3 = moderate swelling and erythema extending from the ankle to tarsus, 4 = severe swelling, and erythema encompassing the foot, ankle, and digits, or ankylosis of the limb.[21] The paw scores were summed for each limb of every mouse with a maximum score of 16 per mouse. The bilateral hind paw thickness (mm) was measured by a caliper. The first administration was performed at 30 days after the primary immunization. On the day, the experimental arthritis had already started. The paws of animals randomly appeared to be mild red and swollen, and average of the clinical scores of the CIA mice was a little bit more than 1.

2.10 Histopathological and immunofluorescence analyses

All the mice were sacrificed at 3 days after the last injections. For histopathological analyses, the knee joints were collected and then fixed in 4% (*W*/*V*) PBS-buffered paraformaldehyde overnight, and decalcified using 10% (*W*/*V*) EDTA solution for 28 days. Subsequently, the joints were embedded in paraffin and sliced into 5 mm thickness for hematoxylin and eosin (H&E) staining and immunofluorescence analyses (TNF-α, IL-1β, and IL-6). The histopathological alterations were detected by a microscope (Nikon Eclipse *Ti*, Optical Apparatus Co., Ardmore, PA, USA) with 10 × eyepiece, 4 × objective for full view of knee joints, and 10 × objective for analyses by histopathological scores of synovium (HSS) to measure synovitis status (Table S1, ESI†)[22,23] and modified Osteoarthritis Research Society International (OARSI) scores to assess articular cartilage status (Table S2, ESI†).[22,23] Immunofluorescence was detected by a LSM 780 CLSM (Carl Zeiss, Jena, Germany) with 10 × eyepiece and 10 × objective. In addition, the relative positive areas of pro-inflammation cytokines were measured by ImageJ software (National Institutes of Health, Bethesda, Maryland) for semiquantitative analyses.

Table 1 Primer sequences for RT-PCR

Gene	Forward Primer (5' to 3')	Reverse Primer (5' to 3')
TNF-α	TATGGCTCAGGGTCCAACTC	GGAAAGCCCATTTGAGTCCT
IL-1β	CTCACAAGCAGAGCACAAGC	CAGTCCAGCCCATACTTTAGG
IL-6	CGGAGAGGAGACTTCACAGAG	CATTTCCACGATTTCCCAGA
GADPH	AGAGAGGGAGGAGGGGAAATG	AACAGGGAGGAGCAGAGAGCAC

2.11 Real-time reverse transcriptase polymerase chain reaction (RT-PCR) tests

The total RNA of affected joints isolated from sacrificed mice of all groups was extracted. The affected joints were grinded into powder in liquid nitrogen. And then, TRIzol reagent (Thermo Fisher Scientific Inc., Shanghai, P. R. China) was added. After extraction, purification, and drying, the RNA concentration of every sample was detected, and then the reverse transcription kit was used for conversion of complimentary DNA (cDNA) according to the manufacturer's instructions. The application of SYBR Premix Ex Taq™ kit according to the protocol was subsequently performed, and RT-PCR was finally performed on a Stratagene Mx3005P system (Stratagene, La Jolla, CA, USA). As shown in Table 1, the primers of TNF-α, IL-1β, and IL-6 were specifically designed and housekeeping gene GADPH was also showed. ΔΔCt method was applied for result analyses.

2.12 ELISA assays

Serum samples were obtained at 48 days after the primary immunization. The levels of TNF-α, IL-1β, and IL-6 in serum were determined using ELISA kits according to the manufacturer's instructions.

2.13 Statistical analyses

Statistical analyses of all experimental data were performed at least three times and expressed as mean ± standard deviation (SD). Statistical significance of data was calculated by using SPSS 14.0 (SPSS Inc., Chicago, IL, USA). $P < 0.05$ was considered statistically significant, and $P < 0.01$ and $P < 0.001$ were considered highly significant.

3 Results and discussion

3.1 Syntheses and characterizations of conjugates

As shown in Scheme 1, Dex-*g*-MTX/FA and Dex-*g*-MTX were prepared through condensation reaction between the hydroxyl groups in Dex and carboxyl groups in MTX and/or FA. The chemical structures were confirmed by ^{1}H NMR and FT-IR spectra. As shown in Fig. 1, the peaks appeared at 5.2 – 4.5 and 3.9 – 3.2 ppm were assigned to Dex, and the peaks at 6.84 ppm (a), 7.64 ppm (b), and 8.53 ppm (c) were belonged to the aromatic protons of MTX and FA. The successful syntheses of Dex-*g*-MTX/FA and Dex-*g*-MTX were also demonstrated by FT-IR spectra as shown in Fig. S1 (ESI†). The absence of the characteristic peaks at 1605 and 1640 cm^{-1} attributed to carboxyl group in MTX or FA, and the appearance of signal of 1599 cm^{-1}assigned to the carbonyl group in prodrug on the FT-IR spectra of Dex-*g*-MTX/FA and Dex-*g*-MTX meant the successful reaction between Dex and MTX or FA. The MTX contents of Dex-*g*-MTX/FA and Dex-*g*-MTX were respectively detected to be 3.7 and 4.2 wt.% through standard curve method on a UV-Vis spectrophotometer. The FA content of Dex-*g*-MTX/FA was calculated to be 1.6 wt.%.

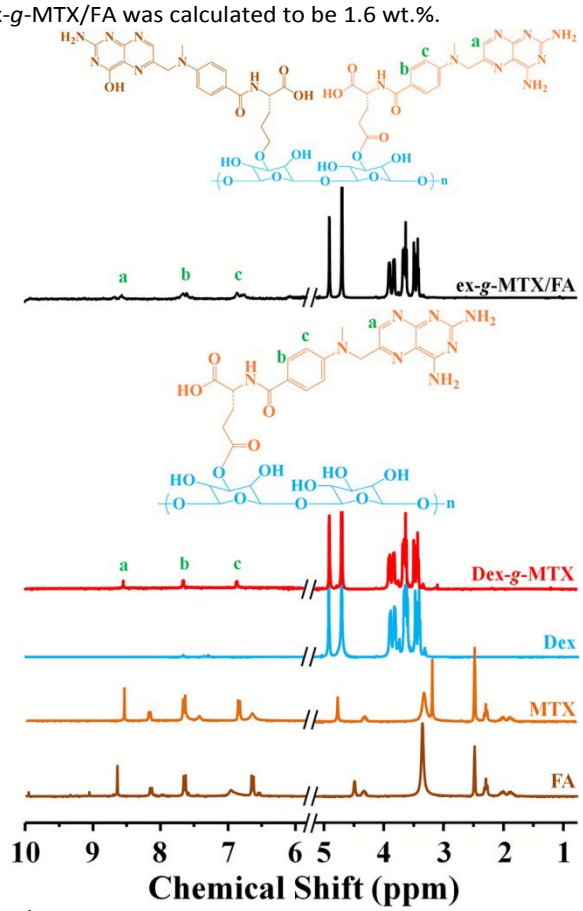

Fig. 1 ^{1}HNMR spectra of Dex-*g*-MTX/FA, Dex-*g*-MTX, and Dex in D_2O, and MTX and FA in DMSO-d_6.

Both Dex-*g*-MTX/FA and Dex-*g*-MTX on account of hydrophilic Dex and hydrophobic MTX and/or FA possessed amphiphilic property. In aqueous environment, the two conjugates self-assembled into micelles exhibiting spherical morphology, which was confirmed by TEM as shown in Fig. 2A and 2C. The apparent mean diameters of Dex-*g*-MTX/FA and Dex-*g*-MTX measured from TEM microimages were both about 90 nm. As shown in Fig. 2B and 2D, the hydrodynamic diameters (D_hs) of Dex-*g*-MTX/FA and Dex-*g*-MTX micelles determined by DLS were 82.4 ± 8.82 and 95.0 ± 18.14 nm, respectively, which were similar with TEM results. The diameters of the two prodrug micelles at about 90 nm were appropriate for passive targeting accumulation in lesion site *via* the enhanced permeation and retention (EPR) effect.[24–26] In fact, the nanoparticles with the sizes over 200 nm will be eliminated by spleen, and the ones with the sizes smaller than 10 nm can be rapidly penetrated by the kidney's filtration system.[27] The nanoparticles with the scales ranged from 45 to 115 nm in size were suitable for drug delivery through intravenous administration toward experimental arthritis animal models attributed to the optimal EPR effects.[28] Consequently, nanoparticles with an appropriate size can provide long-circulating kinematics, which can upregulate selective accumulation and deliver drugs to the desirable sites.

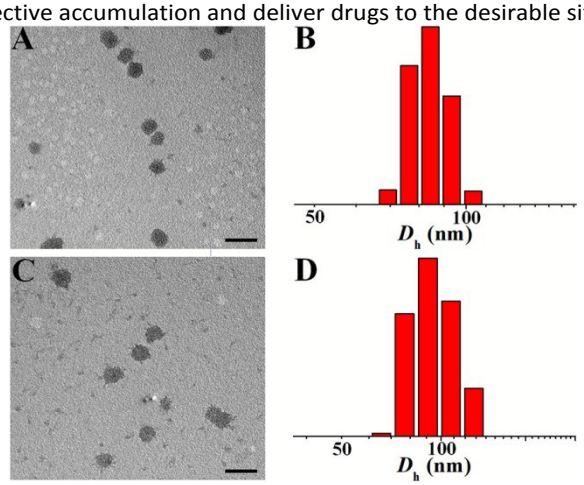

Fig. 2 Typical TEM microimages (A and C) and D_hs (B and D) of Dex-*g*-MTX/FA (A and B) and Dex-*g*-MTX (C and D). Scale bars: 500.0 nm.

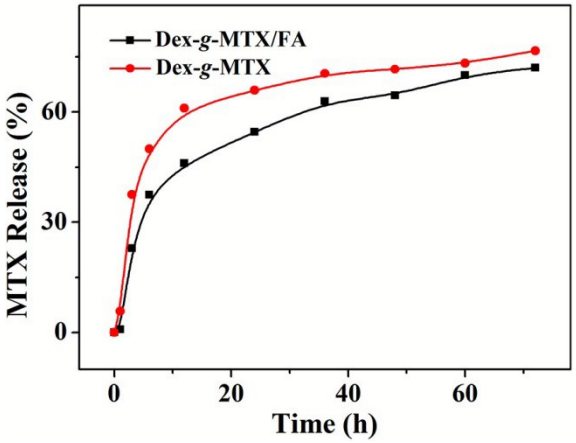

Fig. 3 MTX release from Dex-*g*-MTX/FA and Dex-*g*-MTX in PBS of pH 7.4 at 37 °C.

The CMCs of Dex-*g*-MTX/FA and Dex-*g*-MTX were measured by fluorophotometry with Nile Red as a probe. The prodrug concentration at the first inflection point in the sigmoidal curve was defined as CMC. As shown in Fig. S2, ESI†, the CMCs of Dex-*g*-MTX/FA and Dex-*g*-MTX were determined to be 5.84 × 10^{-2} and 0.21 mg/mL, respectively. The distinction of CMCs between Dex-*g*-MTX/FA and Dex-*g*-MTX was attributed to the content of hydrophobic moiety. Because Dex-*g*-MTX/FA possessed more hydrophobic group composed of MTX and FA, the concentration for self-assembly into micelle

was lower than that of Dex-*g*-MTX. The above results were clearly proved that the two conjugates would self-assemble into micelles in aqueous solution.

Biocompatibility for a newly designed nanomedicine is remarkable characteristic, which is conclusive for application in clinic.[29,30] Hemolysis assay as a common approach is widely used for evaluating the biocompatibility of nanomedicine. Hemolysis is invariably given rise to a multitude of physical and chemical factors and toxins, which subsequently leads to the destruction of RBCs and the release of hemoglobin. Negative hemolysis is a primary condition for venous administration of nanomedicine. In this work, the biocompatibility of Dex-*g*-MTX/FA and Dex-*g*-MTX was assessed by a hemolysis assay through spectroscopy according to the previously reported approach.[31] As shown in Fig. S3 (ESI†), it was manifested that Dex-*g*-MTX/FA, Dex-*g*-MTX, and free MTX, all had no hemolysis in all concentrations. Therefore, the results proved that the two conjugates possessed favorable biocompatible properties and could be applied *via* intravenous administration.

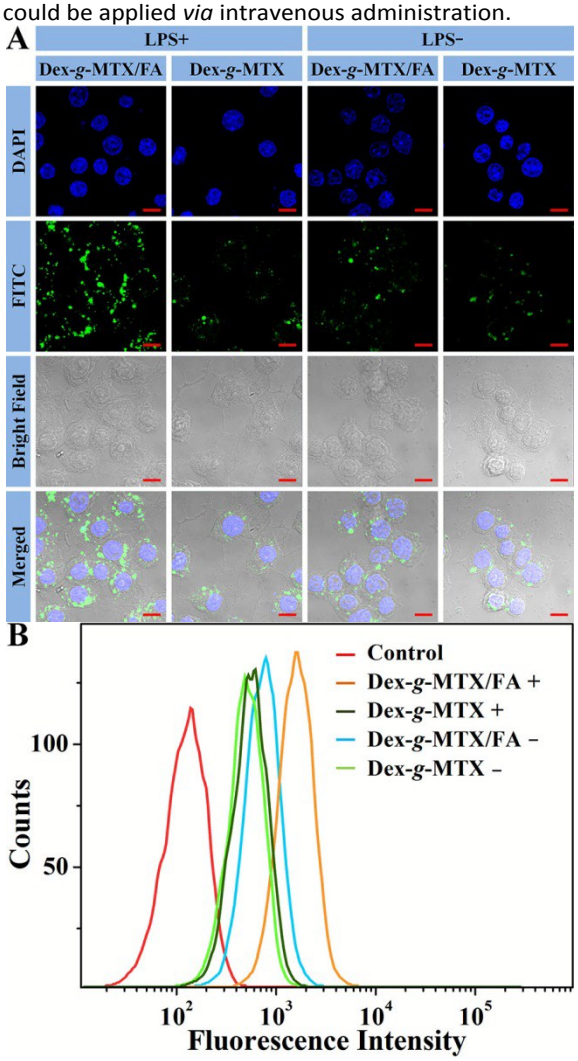

Fig. 4 CLSM microimages (A) and FCM results (B) of RAW 264.7 cells incubated with FITC-Dex-*g*-MTX/FA or FITC-Dex-*g*-MTX for 2 h after activation by LPS (+) or not (–). Scale bars: 10.0 μm.

3.2 *In vitro* drug release, and upregulated cellular uptake and cytotoxicity of Dex-*g*-MTX/FA

The release behaviors of MTX from Dex-*g*-MTX/FA and Dex-*g*-MTX were detected in PBS at pH 7.4. As shown in Fig. 3, no significant burst release of MTX was observed from both Dex-*g*-MTX/FA and Dex-*g*-MTX. The release profiles of MTX from Dex-*g*-MTX/FA and Dex-*g*-MTX were almost the same. In detail, the release speed of MTX from Dex-*g*-MTX/FA was a little slower than that from Dex-*g*-MTX. Finally, 72.04 and 77.68% of loaded MTX were respectively released from Dex-*g*-MTX/FA and Dex-*g*-MTX. The reason might be that the hydrophobic moieties of Dex-*g*-MTX/FA were more than that of Dex-*g*-MTX because of the extra FA, which leaded to more barriers against MTX release from the core of prodrug micelle. Therefore, the speed of MTX release from Dex-*g*-MTX/FA was slower than that from Dex-*g*-MTX.

The activated macrophages are a primary target for RA therapy due to their significant contribution in RA progress and joint destruction. To demonstrate the targeting characteristic of Dex-*g*-MTX/FA *in vitro*, the cellular uptake of Dex-*g*-MTX/FA and Dex-*g*-MTX labeled by FITC was assessed by both CLSM and FCM toward the activated and nonactivated RAW 264.7 cells. As shown in Fig. 4A, compare to FITC-Dex-*g*-MTX, higher fluorescence intensity was detected in the FITC-Dex-*g*-MTX/FA-cocultured activated RAW 264.7 cells with overexpressed FR. However, there is little distinction between FITC-Dex-*g*-MTX/FA and FITC-Dex-*g*-MTX cocultured with the nonactivated RAW 264.7 cells.

To further confirm the cellular uptakes and active targeting properties of Dex-*g*-MTX/FA towards the activated macrophages, FCM was performed then. As shown in Fig. 4B, it was clearly demonstrated that the activated RAW 264.7 cells cultured with FITC-Dex-*g*-MTX/FA had the highest fluorescence intensity in all groups. Moreover, the fluorescence intensity of FITC-Dex-*g*-MTX in the activated RAW 264.7 cells was nearly to those of FITC-Dex-*g*-MTX/FA and FITC-Dex-*g*-MTX in the nonactivated RAW 264.7 cells. As similar with CLSM, the fluorescence intensity of FITC-Dex-*g*-MTX in the nonactivated RAW 264.7 cells was much closed to that of FITC-Dex-*g*-MTX/FA.

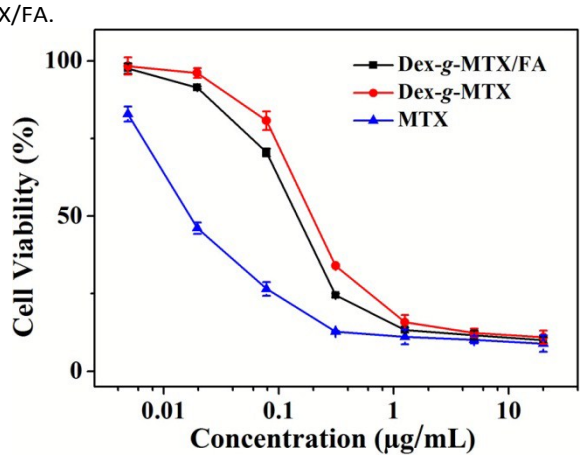

Fig. 5 Cytotoxicity of Dex-*g*-MTX/FA, Dex-*g*-MTX, and free MTX after coincubation for 72 h toward RAW 264.7 cells activated by LPS *in vitro*. Data were presented as a mean ± SD (n = 3).

To confirm the cytotoxicity of the two conjugates, MTT assay was carried out toward the activated RAW 264.7 cells. As shown in Fig. 5, along with the decrease of MTX equivalent concentration of all MTX formulations, the cell proliferation was obviously improved. A little higher inhibition of cell proliferation was demonstrated in Dex-*g*-MTX/FA group in comparison to Dex-*g*-MTX. It might be attributed that more

cellular uptake was conducted by the high affinity of FA in Dex-*g*-MTX/FA to FR overexpressed on the activated RAW 264.7 cells. Interestingly, with the decrease of MTX concentration, free MTX possessed a higher level of toxicity than the two conjugates. It might result from that the broken speed of the ester bond in the two conjugates was slow, and the dissociative MTX for entry into the cells was not enough.

The above results indicated that the two conjugates were almost identical for the nonactivated RAW 264.7 cells on account of the little expression of FR on the nonactivated cells. However, the fluorescence intensity of FITC-Dex-*g*-MTX/FA was increased in the wake of more FR expressed on the activated cells. The results were similar with those of a previous report, that is, a FITC-labeled FA-conjugated dendrimer effectively bound to FR-expressing macrophages, while the internalization of control conjugate without FA was less in the same cells.[6] It illustrates that the high affinity of FA bounding to FR can subsequently lead to the augment of cellular uptake.

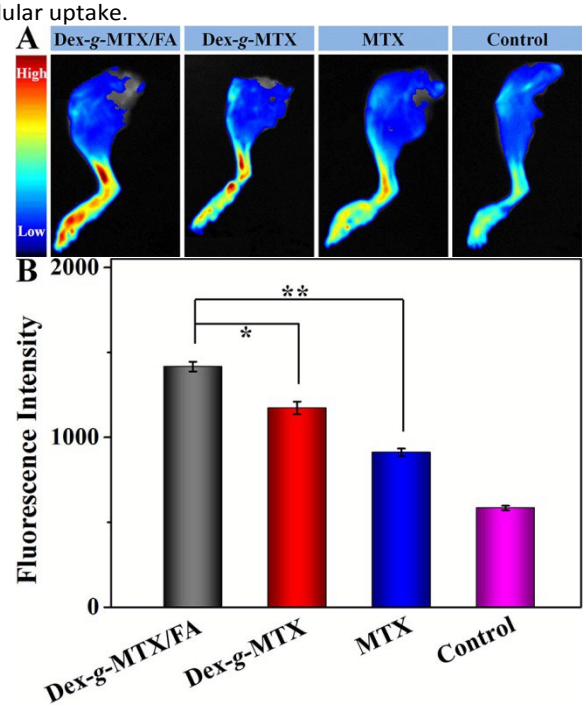

Fig. 6 *Ex vivo* FITC fluorescence images of affected joints (A) and average signals detected from the ankle joints (B) from CIA mice treated with Dex-*g*-MTX/FA, Dex-*g*-MTX, free MTX, or NS as control. Data were presented as mean ± SD (n = 2; **P* < 0.05, ***P* < 0.01).

3.3 Selective biodistribution of Dex-*g*-MTX/FA

The targetability and selective biodistribution as the main consideration in the designation of nanomedicine are important for therapeutic efficacy and adverse effects. To measure the above two properties, the *ex vivo* fluorescence images of isolated hind legs at 12 h post-injection were monitored in CIA mice. As shown in Fig. 6A, the strongest fluorescence intensity signal was detected in the affected joints of CIA mice treated with FITC-Dex-*g*-MTX/FA due to the passive and active targeting properties, whereas the lowest signals were observed in the NS-treated mice. The fluorescence intensity in CIA mice of FITC-Dex-*g*-MTX and FITC-MTX groups were between those of the groups of FITC-Dex-*g*-MTX/FA and NS. Compared with FITC-MTX, a higher fluorescence signal was detected in CIA mice injected with FITC-Dex-*g*-MTX because of selective accumulation through the EPR effect. In addition, the promising targetability of Dex-*g*-MTX/FA was further semi-quantatively proved as shown in Fig. 6B. The result clearly revealed that the fluorescence intensity of FITC-Dex-*g*-MTX/FA group was almost 1.2, 1.6, and 2.5 times higher than that in the FITC-Dex-*g*-MTX, FITC-MTX, and NS-treated mice, respectively. Although nontargeted conjugate of Dex-*g*-MTX exhibited a certain amount of selectivity for the EPR effect, the ideal biodistribution was obviously observed in the Dex-*g*-MTX/FA group by its additional active targetability *via* a high affinity to FR overexpressed on the activated macrophages. These results suggested that Dex-*g*-MTX/FA possessed high targetability for the affected joints in CIA mice and great potential for RA therapy.

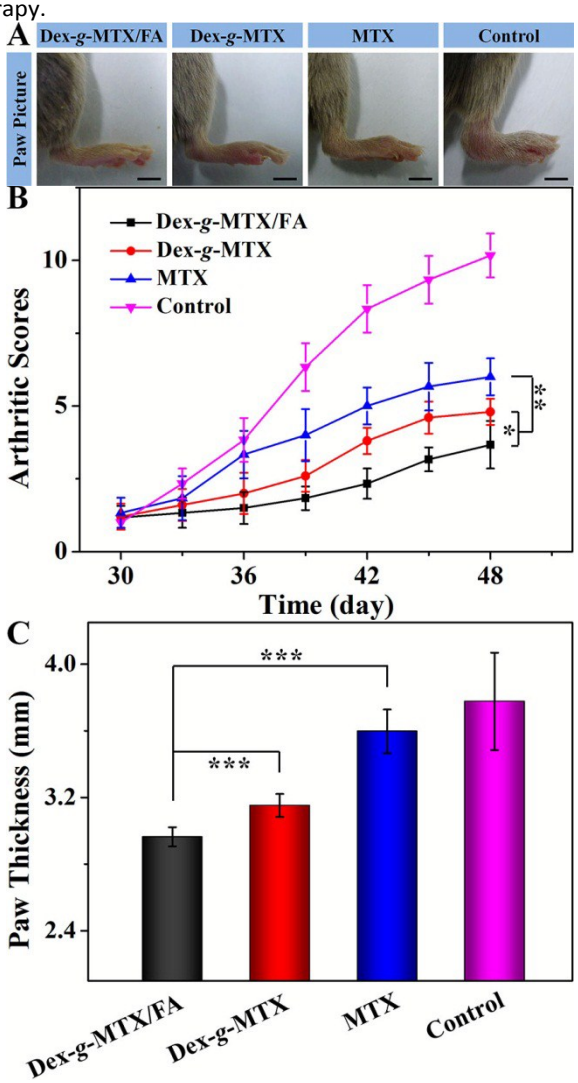

Fig. 7 Macroscopic images of inflamed joints from CIA mice treated with Dex-*g*-MTX/FA, Dex-*g*-MTX, free MTX, or NS as control after 3 days of last injection (A). The macroscopic evidences of arthritis were assessed by arthritic sores in the process of treatment (B) and paw thickness after all treatments (C). Data were presented as mean ± SD (n = 6; **P* < 0.05, ***P* < 0.01, ****P* < 0.001). Scale bars: 5.0 mm.

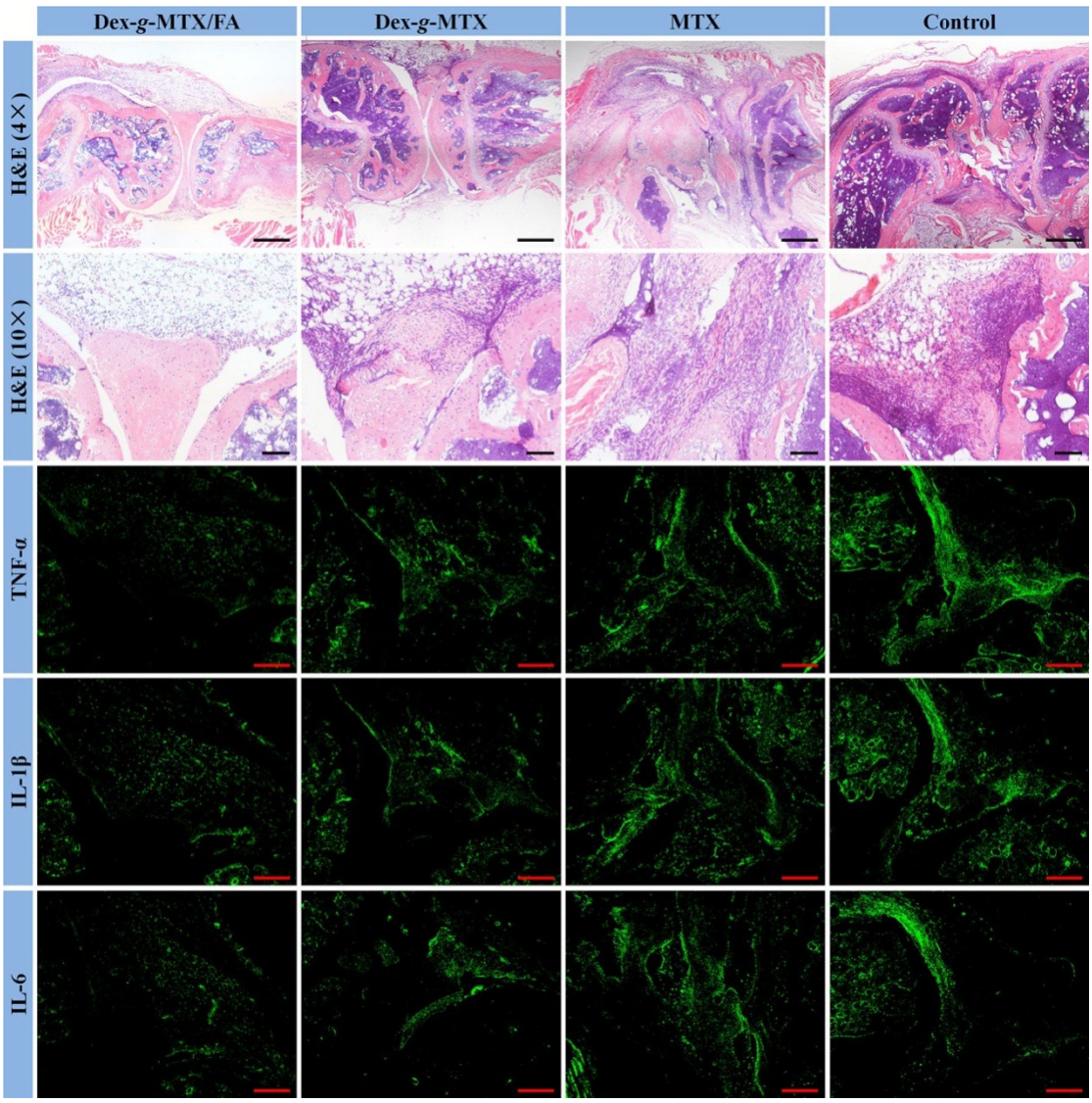

Fig. 8 Microimages of H&E staining and immunofluorescence analyses (*i.e.*, TNF-α, IL-1β, and IL-6) of affected joints using continuous sections. Scale bars in H&E (4×): 500.0 μm; scale bars in H&E (10×) and immunofluorescence: 200.0μm.

3.4 Enhanced therapeutic efficacies of targeted prodrug

The therapeutic efficacy of a new drug in animal model is the most important assessment index. In this work, CIA mouse model acted as the most common animal model for RA was applied according to the previously published approach.[21] To evaluate the anti-inflammation effects, the CIA mice were treated with Dex-*g*-MTX/FA, Dex-*g*-MTX, and free MTX at a MTX equivalent dose of 5 mg/(kg BW), and NS as control *via* venous administration once every 3 days, which initiated at 30 days after the primary immunization (Scheme 2). At this time, the CIA had begun, and the clinical scores of every group were approached around 1 as shown in Fig. 7B. As shown in Fig. 7A, the hind paw images of all groups were taken at 48 days after the primary immunization. It was clearly demonstrated that whether the two conjugates or free MTX could suppress the erythema and swelling of inflamed joints to various degrees. As our expectation, the most potent inflammation inhibition was obtained in the CIA mice treated with Dex-*g*-MTX/FA compared with nontargeted conjugate and free drug. As shown in Fig. 7B, the arthritic sores were monitored at 3 days after every intravenous injection. The arthritic score of Dex-*g*-MTX/FA group was grew slowly and approached to 3.7 at 3 days after the last administration, which was significantly lower than those of Dex-*g*-MTX (*i.e.*, 4.8) and free MTX group (*i.e.*, 6.0) ($P < 0.05$ and $P < 0.01$, respectively). However, a rapid increase of arthritic score was clearly observed in control group during the whole treatment course, and the arthritic score was reached to 10.2 at the last measurement eventually. Therefore, it was obviously suggested that the most remarkable suppression of clinical score was obtained in the CIA mice treated with Dex-*g*-MTX/FA. The most effective therapeutic outcome might be attributed to the high passive and active targetability of Dex-*g*-MTX/FA. Logically, the arthritic inflammation of CIA mice treated with Dex-*g*-MTX was moderately inhibited compared with that administrated with Dex-*g*-MTX/FA, because of the nonactive targetability of Dex-*g*-MTX. To objectively assess the therapeutic efficacies of various MTX formulations, the hind paw thickness as an indicator of arthritis symptom was measured at 3 day after the last intravenous injection, as shown in Fig. 7C The average hind paw thicknesses of Dex-*g*-MTX/FA, Dex-*g*-MTX, free MTX, and control group were 2.96, 3.15, 3.60, and 3.78 mm, respectively.

It was visually showed that the best therapeutic efficacy was obtained by the administration of Dex-*g*-MTX/FA in keeping with the results of clinical scores.

To further confirm the therapeutic efficacies of the conjugates, the histopathological and immunofluorescence analyses were the key procedures to be carried out. As shown in Fig. 8, in the H&E staining microimages of the joint of NS-treated mouse, a multitude of inflammation cells stained blue by hematoxylin infiltrated in hyperplastic synovium. The articular cartilage invaded in abundance by the production of a plenty of pro-inflammation cytokines and proteases became increasingly rough and thin. Meanwhile, the joint space became severely narrow. Whereas, the microscopic histopathological microimages of Dex-*g*-MTX/FA group suggested that a few inflammation cells infiltrated in the affected joints, and the morphology of articular cartilage was integral due to a little hyperplasia of synovium. Although the administration of Dex-*g*-MTX could approximately maintain the smooth and integrity of articular cartilage, the mild infiltration of inflammation cells and hyperplasia of synovium were clearly exhibited. As listed in Tables S1 and S2, ESI†, the following HSS and OARSI score analyses could further illustrate the results. As shown in Fig. 9A and 9B, some effects on the inhibition of synovitis and cartilage destruction were detected *via* free MTX. More fascinatingly, the groups of the two MTX prodrugs, that is, Dex-*g*-MTX/FA and Dex-*g*-MTX, exhibited efficient suppression of synovium inflammation and protection against articular cartilage erosion. Moreover, a better efficacy was demonstrated in the group of Dex-*g*-MTX/FA attributed to the active targetability toward FR and selective biodistribution in the affected joints.

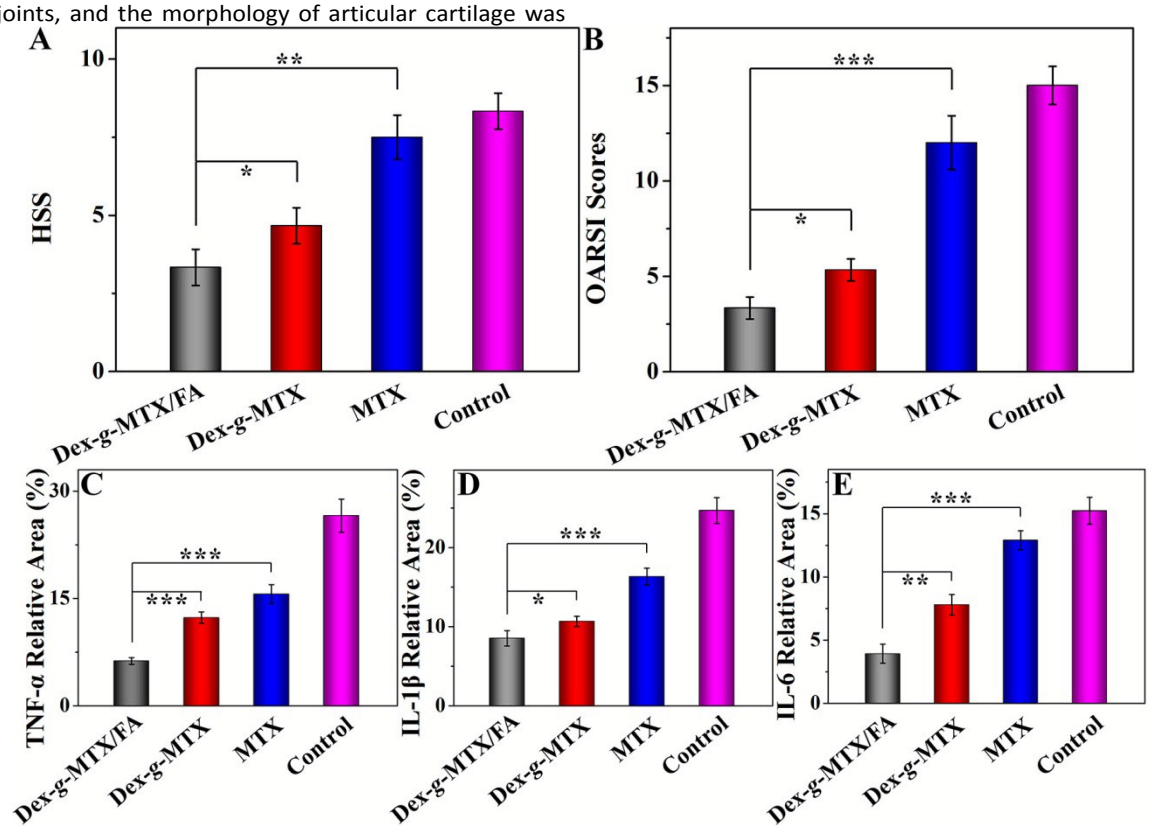

Fig. 9 Histopathological scores of synovium (HSS) (A) and modified OARSI scores (B) of Dex-*g*-MTX/FA, Dex-*g*-MTX, free MTX, and NS as control groups determined by microimages of H&E staining. Relative positive areas of proinflammatory cytokines, *i.e.*, TNF-α (C), IL-1β (D), and IL-6 (E), calculated by ImageJ software. Data were presented as mean ± SD (n = 3; *P < 0.05, **P < 0.01, ***P < 0.001).

The levels of proinflammatory cytokines in the affected joints are the key indicators of disease severity, such as TNF-α, IL-1β, and IL-6.[32–36] Among numerous proinflammatory cytokines, TNF-α mainly derived from the activated macrophages in the synovium is a crucial factor for the induction of other proinflammatory cytokine release and joint damage.[37] Another important proinflammatory cytokine in the pathogenesis of RA is IL-1β. It is a member of IL-1, which is correlated with the synovitis and articular damage. Importantly, it was reported that the induction factor of RA synovitis was the combination of TNF-α with IL-1β.[38] IL-6 is implicated in the activation of synovial fibroblasts and osteoclasts subsequently resulting in articular cartilage and bone erosion.[39,40] Consequently, the immunofluorescence of the continuous sections of inflamed joints was performed in order to ulteriorly determine the change of inflammatory condition and better illustrate the expression of the inflammatory cytokines in the affected joints. As shown in Fig. 8, the expression areas of most inflammatory cytokines were located in hyperplastic synovium, corresponding to the areas of infiltrated inflammatory cells in the H&E staining microimages. Reasonably, the most remarkable reduction of the expression of TNF-α, IL-1β, and IL-6 in the affected joint of Dex-*g*-MTX/FA group was demonstrated. In addition, the expression of TNF-α, IL-1β, and IL-6 in the inflamed joints of Dex-*g*-MTX and free MTX groups was down-regulated in different degrees. Whereas, the significant increase of the secretion of TNF-α, IL-1β, and IL-6 was discovered in the joint

of NS-treated mice. To further confirm it, the relative expression area of the above three proinflammatory cytokines was analyzed with ImageJ software. The relative expression areas of TNF-α, IL-1β, and IL-6 were calculated as the follow sequence: NS > free MTX > Dex-*g*-MTX > Dex-*g*-MTX/FA. As shown in Fig. 9C, the TNF-α relative expression of Dex-*g*-MTX/FA group was 6.27%, which was far lower than those of Dex-*g*-MTX, *i.e.*, 12.31% ($P < 0.001$), and free MTX group, *i.e.*, 15.61% ($P < 0.001$). As shown in Fig. 9D and 9E, a similarly inhibited pattern was demonstrated. The relative expression area of IL-1β and IL-6 of Dex-*g*-MTX/FA group was 8.52 and 3.92%, respectively, which were significantly smaller than those of Dex-*g*-MTX and free MTX groups.

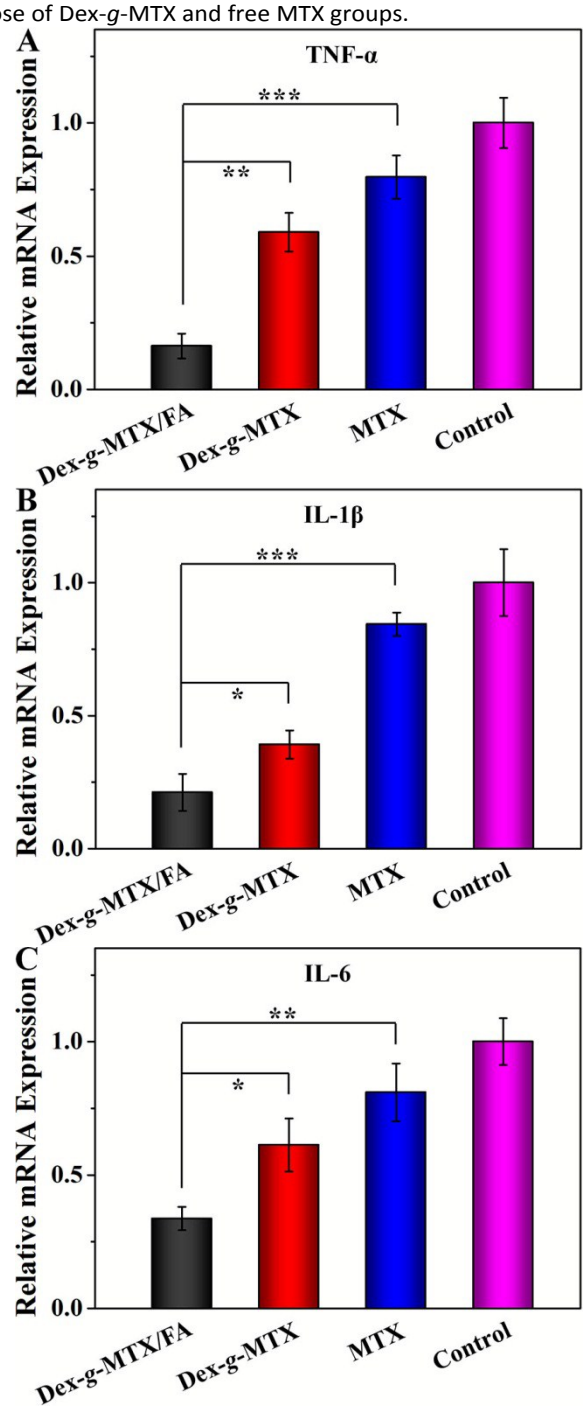

Fig. 10 Relative mRNA expression of proinflammatory cytokines, *i.e.*, TNF-α (A), IL-1β (B), and IL-6 (C), in Dex-*g*-MTX/FA, Dex-*g*-MTX, free MTX, and NS as control groups. Data were presented as mean ± SD ($n = 3$; *$P < 0.05$, **$P < 0.01$, ***$P < 0.001$).

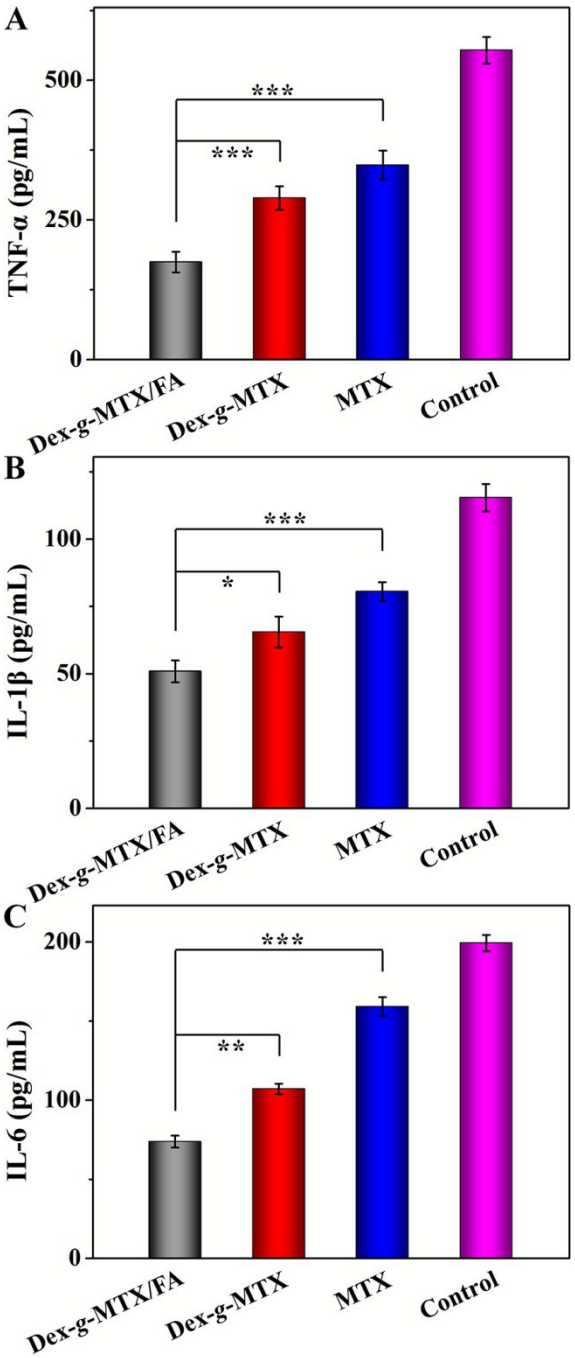

Fig. 11 Serum concentrations of proinflammatory cytokines, *i.e.*, TNF-α (A), IL-1β (B), and IL-6 (C), in Dex-*g*-MTX/FA, Dex-*g*-MTX, free MTX, and NS as control groups measured by ELISA tests. Data were presented as mean ± SD ($n = 3$; *$P < 0.05$, **$P < 0.01$, ***$P < 0.001$).

To further reveal the inhibition efficacies of various MTX formulations toward the proinflammatory cytokines *in situ*, the relative mRNA expression of TNF-α, IL-1β, and IL-6 in the hyperplastic synovium was detected by RT-PCR tests. As shown in Fig. 10, the inflamed joints of Dex-*g*-MTX/FA group exhibited the lowest relative mRNA expression of three proinflammatory cytokines among all groups. The results combined with those of immunofluorescence illustrated that Dex-*g*-MTX/FA could

significantly down-regulate the expression of proinflammatory cytokines due to selective accumulation in the wanted location through the favorable targetability of Dex-*g*-MTX/FA toward the activated macrophages, which were acted as a main source of proinflammatory cytokines. Therefore, it was indicated that the same trend of therapeutic efficacy of different MTX formulations was confirmed again.

Furthermore, the levels of proinflammatory cytokines in serum are the significant indicators of therapeutic efficacy. The concentrations of proinflammatory cytokines in serum are implicated in the severity of joint inflammation in experimental arthritis. Consequently, to explore the impacts of different MTX formulations on serum levels of proinflammatory cytokines, the serum concentrations of TNF-α, IL-1β, and IL-6 were determined. As shown in Fig. 11, the concentrations of the three proinflammatory cytokines, TNF-α, IL-1β, and IL-6, were remarkably increased in the serum of NS-treated CIA mice. In all the three treatment groups, the concentrations of proinflammatory cytokines were decreased in different degrees. The serum concentration of Dex-*g*-MTX/FA group was almost 1.7 and 2.0 times ($P < 0.001$) in TNF-α, 1.3 ($P < 0.05$) and 1.6 times ($P < 0.001$) in IL-1β, and 1.5 ($P < 0.01$) and 2.2 times ($P < 0.001$) in IL-6 lower than those of Dex-*g*-MTX and free MTX groups, respectively. It followed that more significant reduction of the proinflammatory cytokines concentration was detected in the Dex-*g*-MTX/FA group compared with the group of Dex-*g*-MTX due to its high affinity to FR overexpressed on the activated macrophages in hyperplastic synovium. It was reported that some MTX nanoformulations, such as the hyaluronic acid–methotrexate (HA–MTX) conjugate[41] and the MTX-loaded arginine-glycine-aspartic acid (RGD)-conjugated poly(DL-lactide-*co*-glycolide) Au half-shell nanoparticle[42] exhibited effective inhibition of synovitis and cartilage erosion, and remarkably suppressed production of proinflammatory cytokines systemically and locally. Similarly, according to the results stated above, the designed conjugate, *i.e.*, Dex-*g*-MTX/FA, not only notably inhibited synovitis in the affected joints, but also observably protected articular cartilage and bone against erosion and destruction through effective suppression of the production of proinflammatory cytokines.

4 Conclusions

In this work, the macrophages-targeted Dex-*g*-MTX/FA and nontargeted Dex-*g*-MTX as control were synthesized for the targeted therapy of RA. The two conjugates assembled into micelles in aqueous environment with a diameter of around 90 nm, which was suitable for selective passive accumulation in the affected joints through the EPR effect and beneficial to obtain the excellent therapeutic efficacy.[28] Furthermore, FA as a targeted group was bond to Dex-*g*-MTX for more directional drug delivery. Importantly, the significant suppression of inflammation was achieved *via* intravenous administration of Dex-*g*-MTX/FA due to the targetability of FA, selective accumulation, and reduction of proinflammatory cytokine production. Meanwhile, the significant suppression of synovitis and effective protection of articular cartilage were exhibited in the Dex-*g*-MTX/FA group by inhibition of expression and secretion of proinflammatory cytokines. Consequently, the all above results suggested that the macrophage-targeted prodrug, that is, Dex-*g*-MTX/FA, possessed favorable potential for targeted therapy of RA.

It follows that the cell-targeted nanomedicine in abnormal synovium in RA will obtain excellent clinical outcome. In the future, nanomedicine with high targetability, which can biologically excise hyperplastic synovium, may prevent RA patients from articular cartilage and bone erosion, and even joint replacement.

Acknowledgements

This research was financially supported by National Natural Science Foundation of China (Nos. 81171681, 51303174, 51233004, 51390484, 51321062, 51473165, 51203153, and 51273196), National Science Foundation for Post-Doctoral Scientists of China (No. 2013M530990), and Scientific Development Program of Jilin Province (Nos. 20140520050JH and 20130206058GX).

Notes and references

1 I. B. McInnes and J. R. O'Dell, *Ann. Rheum. Dis.*, 2010, **69**, 1898–1906.
2 D. L. Scott, F. Wolfe and T. W. Huizinga, *Lancet*, 2010, **376**, 1094–1108.
3 I. B. McInnes and G. Schett, *New Engl. J. Med.*, 2011, **365**, 2205–2219.
4 R. W. Kinne, B. Stuhlmuller and G. R. Burmester, *Arthritis Res. Ther.*, 2007, **9**, 224.
5 R. Qi, I. Majoros, A. C. Misra, A. E. Koch, P. Campbell, H. Marotte, I. L. Bergin, Z. Cao, S. Goonewardena, J. Morry, S. Zhang, M. Beer, P. Makidon, A. Kotlyar, T. P. Thomas and J. R., Jr. Baker, *J. Biomed. Nanotechnol.*, 2015, **11**, 1431–1441.
6 T. P. Thomas, S. N. Goonewardena, I. J. Majoros, A. Kotlyar, Z. Cao, P. R. Leroueil and J. R., Jr. Baker, *Arthritis Rheum.*, 2011, **63**, 2671–2680.
7 U. Bilthariya, N. Jain, V. Rajoriya and A. K. Jain, *Drug Dev. Ind. Pharm.*, 2015, **41**, 95–104.
8 S. H. Kim, J. H. Kim, D. G. You, G. Saravanakumar, H. Y. Yoon, K. Y. Choi, T. Thambi, V. G. Deepagan, D. G. Jo and J. H. Park, *Chem. Commun.*, 2013, **49**, 10349–10351.
9 J. L. Davignon, M. Hayder, M. Baron, J. F. Boyer, A. Constantin, F. Apparailly, R. Poupot and A. Cantagrel, *Rheumatology*, 2013, **52**, 590–598.
10 A. C. Antony, *Annu. Rev. Nutr.*, 1996, **16**, 501–521.
11 N. Nakashima-Matsushita, T. Homma, S. Yu, T. Matsuda, N. Sunahara, T. Nakamura, M. Tsukano, M. Ratnam and T. Matsuyama, *Arthritis Rheum.*, 1999, **42**, 1609–1616.
12 P. S. Low, W. A. Henne and D. D. Doorneweerd, *Accouts Chem. Res.*, 2008, **41**, 120–129.
13 B. J. Crielaard, T. Lammers, R. M. Schiffelers and G. Storm, *J. Control. Release*, 2012, **161**, 225–234.
14 R. Qi, I. Majoros, A. C. Misra, A. E. Koch, P. Campbell, H. Marotte, I. L. Bergin, Z. Cao, S. Goonewardena and J. Morry, *J. Biomed. Nanotechnol.*, 2015, **11**, 1431–1441.
15 L. K. Prasad, H. O'Mary and Z. Cui, *Nanomedicine*, 2015, **10**, 2063–2074.
16 M. Cutolo, A. Sulli, C. Pizzorni, B. Seriolo and R. H. Straub, *Ann. Rheum. Dis.*, 2001, **60**, 729–735.
17 Z. A. Khan, R. Tripathi and B. Mishra, *Expert Opin. Drug Del.*, 2012, **9**, 151–169.
18 A. D. Baldwin and K. L. Kiick, *Biopolymers*, 2010, **94**, 128–140.

19 K. Raemdonck, T. F. Martens, K. Braeckmans, J. Demeester and S. C. De Smedt, *Adv. Drug Deliver. Rev.*, 2013, **65**, 1123–1147.
20 J. Ding, D. Li, X. Zhuang and X. Chen, *Macromol. Biosci.*, 2013, **13**, 1300–1307.
21 D. D. Brand, K. A. Latham and E. F. Rosloniec, *Nat. Protoc.*, 2007, **2**, 1269–1275.
22 H. Liu, J. Ding, J. Wang, Y. Wang, M. Yang, Y. Zhang, F. Chang and X. Chen, *PloS ONE*, 2015, **10**, e0120596.
23 H. Liu, J. Ding, C. Wang, J. Wang, Y. Wang, M. Yang, Y. Jia, Y.Zhang, F. Chang, R. Li and X. Chen, *Tissue Eng. Part A*, 2015, **21**, 2733–2743.
24 V. Torchilin, *Adv. Drug Deliver. Rev.*, 2011, **63**, 131–135.
25 K. Maruyama, *Adv. Drug Deliver. Rev.*, 2011, **63**, 161–169.
26 H. Kobayashi, R. Watanabe and P. L. Choyke, *Theranostics*, 2013, **4**, 81–89.
27 S. Mitragotri and J. W. Yoo, *Arch. Pharm. Res.*, 2011, **34**, 1887–1897.
28 T. Ishihara, T. Kubota, T. Choi and M. Higaki, *J. Pharmacol. Exp. Ther.*, 2009, **329**, 412–417.
29 A. Afshar-Oromieh, A. Malcher, M. Eder, M. Eisenhut, H. G. Linhart, B. A. Hadaschik, T. Holland-Letz, F. L. Giesel, C. Kratochwil, S. Haufe, U. Haberkorn and C. M. Zechmann, *Eur. J. Nucl. Med. Mol. I.*, 2013, **40**, 971–972.
30 C. J. Kirkpatrick, F. Bittinger, M. Wagner, H. Kohler, T. G. van Kooten, C. L. Klein and M. Otto, *P. I. Mech. Eng. H.*, 1998, **212**, 75–84.
31 W. Xu, J. Ding, C. Xiao, L. Li, X. Zhuang and X. Chen, *Biomaterials*, 2015, **54**, 72–86.
32 E. Choy, *Rheumatology,* 2012, **51**, v3–v11.
33 E. H. Choy and G. S. Panayi, *New Engl. J. Med.*, 2001, **344**, 907–916.
34 M. Kapoor, J. Martel-Pelletier, D. Lajeunesse, J. P. Pelletier and H. Fahmi, *Nat. Rev. Rheumatol.*, 2011, **7**, 33–42.
35 B. Bartok and G. S. Firestein, *Immunol. Rev.*, 2010, **233**, 233–255.
36 S. Siebert, A. Tsoukas, J. Robertson and I. McInnes, *Pharmacol. Rev.*, 2015, **67**, 280–309.
37 M. Feldmann and S. R. Maini, *Immunol. Rev.*, 2008, **223**, 7–19.
38 W. B. van den Berg, L. A. Joosten, G. Kollias and F. A. van De Loo, *Ann. Rheum. Dis.*, 1999, **58**, I40–148.
39 G. W. Kim, N. R. Lee, R. H. Pi, Y. S. Lim, Y. M. Lee, J. M. Lee, H. S. Jeong and S. H. Chung, *Arch. Pharm. Res.*, 2015, **38**, 575–584.
40 H. Lee, M. Y. Lee, S. H. Bhang, B. S. Kim, Y. S. Kim, J. H. Ju, K. S. Kim and S. K. Hahn, *ACS Nano*, 2014, **8**, 4790–4798.
41 J. M. Shin, S. H. Kim, T. Thambi, D. G. You, J. Jeon, J. O. Lee, B. Y. Chung, D.-G. Jo and J. H. Park, *Chem. Commun.*, 2014, **50**, 7632–7635.
42 S. M. Lee, H. J. Kim, Y. J. Ha, Y. N. Park, S. K. Lee, Y. B. Park and K. H. Yoo, *ACS Nano*, 2013, **7**, 50–57.

TOC graphic

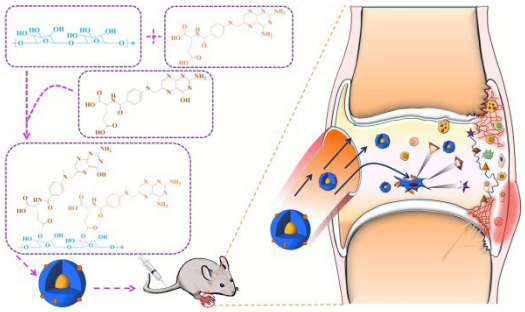

TOC Text

A folate-decorated dextran–methotrexate prodrug is applied for targeted therapy of collagen-induced arthritis in mice.